Inorganic Chemistry

ARTICLE

pubs.acs.org/IC

Edge- versus Vertex-Inversion at Trigonal Pyramidal Ge(II) Centers—A New Aromatic Anchimerically Assisted Edge-Inversion Mechanism

Keith Izod,* Ewan R. Clark, and John Stewart

Main Group Chemistry Laboratories, School of Chemistry, Bedson Building, University of Newcastle, Newcastle upon Tyne, NE1 7RU, U.K.

Supporting Information

ABSTRACT: Theoretical calculations reveal that the model phosphagermylenes {(Me)P(C_6H_4-2-CH_2NMe_2)}GeX [X = F (**1F**), Cl (**1Cl**), Br (**1Br**), H (**1H**), Me (**1Me**)], which are chiral at both the phosphorus and pyramidal germanium(II) centers, may be subject to multiple inversion pathways which result in interconversion between enantiomers/diastereomers. Inversion via a classical vertex-inversion process (through a trigonal planar transition state) is observed for the phosphorus center in all compounds and for the germanium center in **1H**, although this latter process has a very high barrier to inversion (221.6 kJ mol^{-1}); the barriers to vertex-inversion at phosphorus increase with decreasing electronegativity of the substituent X. Transition states corresponding to edge-inversion at germanium (via a T-shaped transition state) were located for all five compounds; for each compound two different arrangements of the substituent atoms [N and X axial (**1**X_{N-X}) or P and X axial (**1**X_{P-X})] are possible, and two distinct transition states were located for each of these arrangements. In the first of these (**1**X_{N-X}^{Planar} and **1**X_{P-X}^{Planar}), inversion at germanium is accompanied by simultaneous planarization at phosphorus; these transition states are stabilized by pπ−pπ interactions between the phosphorus lone pair and the vacant p_z-orbital at germanium. In the alternative transition states (**1**X_{N-X}^{Folded} and **1**X_{P-X}^{Folded}), the phosphorus atoms remain pyramidal and inversion at germanium is accompanied by folding of the phosphide ligand such that there are short contacts between germanium and one of the *ipso*-carbon atoms of the aromatic ring. These transition states appear to be stabilized by donation of electron density from the π-system of the aromatic rings into the vacant p_z-orbital at germanium. The barriers to inversion via **1**X_{P-X}^{Planar} and **1**X_{P-X}^{Folded} are rather high, whereas the barriers to inversion via **1**X_{N-X}^{Planar} and **1**X_{N-X}^{Folded} are similar to those for inversion at phosphorus, clearly suggesting that the most important factor in stabilizing these transition states is the σ-withdrawing ability of the substituents, rather than π-donation of lone pairs or donation of π-electron density from the aromatic rings into the vacant p_z-orbital at germanium.

INTRODUCTION

The dominance of transition metal complexes in stereoselective catalysis is largely built on the successful isolation of enantioenriched or enantiopure chiral ligands, preeminent among which are the tertiary pnictines PnR_3 (Pn = P, As, Sb, Bi).[1] Some of the most useful ligands possess chirality at the pnictogen center itself; in such compounds racemization is slow due to the large barriers to inversion at the pnictogen center (cf. the rapid inversion of tertiary amines).

The inversion behavior of the heavier tertiary pnictines has been studied extensively by both experimental and theoretical means, and there is now a substantial body of information regarding the factors which affect both the barriers to inversion and the inversion mechanisms of these compounds.[2−8] The inversion barriers are significantly affected by (i) steric bulk, (ii) conjugation, and (iii) the electronegativities of the substituents. Sterically bulky substituents tend to confer a less pyramidal conformation at the pnictine center and so typically reduce the barrier to inversion. Similarly, incorporation of the pnictine center into a conjugated (or aromatic) system, either by the addition of vinylic substituents or through the incorporation of the pnictogen center in an unsaturated ring system such as a phosphole, arsole, or stibole, etc., significantly reduces the barrier to inversion; for example, the barriers to inversion at phosphorus for Et_2PH, $(CH_2{=}CH)_2PH$, and phosphole have been calculated as 148.4, 119.6, and 60.4 kJ mol^{-1}, respectively.[2]

The influence of substituent electronegativity has been studied extensively by Mislow and co-workers, who have shown that substitution of a tertiary phosphine by increasingly electropositive EMe_3 groups (E = Si, Ge, Sn) leads to a progressive reduction in the phosphorus inversion barrier.[3] For example, variable-temperature NMR experiments reveal that the free energies of inversion of *i*-PrPhP(EMe_3) are 136.8, 89.5, and 80.8 kJ mol^{-1} for E = C, Ge, and Sn, respectively.[3b] For the limited data set explored, a linear correlation was found between the free energy of inversion and the electronegativity of the substituent atom E in these compounds; a similar correlation was found for tertiary arsines, which have somewhat higher barriers to inversion than their phosphorus analogues. In this regard, it is notable that the combination of the steric bulk and the electropositive nature of the silyl groups in the tertiary phosphine $(i\text{-}Pr_3Si)_3P$ results in a near planar geometry at the phosphorus center, as shown by X-ray crystallography.[4]

Received: January 4, 2011
Published: March 22, 2011

Scheme 1. Inversion Mechanism (Pn = P, As, Sb, Bi)

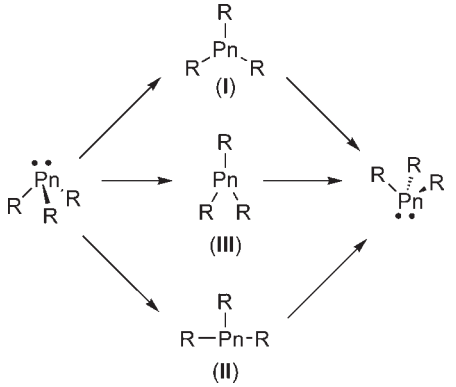

Chart 1

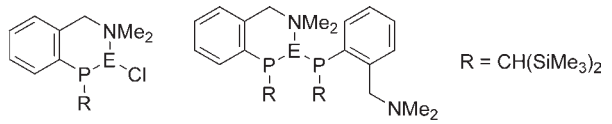

E = Ge (**1**), Sn (**2**) E = Ge (**3**), Sn (**4**)

The foregoing relates to classical inversion via a trigonal planar transition state of essentially D_{3h} symmetry (vertex-inversion (**I**), Scheme 1). However, in 1986 Arduengo and Dixon reported an alternative inversion mechanism which proceeds via a T-shaped transition state of C_{2v} symmetry (edge-inversion (**II**)).[5] This report, along with several subsequent studies by these authors and by others, showed that electronegative substituents favor the latter mechanism; thus, whereas PH_3 and PH_2F are calculated to undergo vertex-inversion, PF_2H and PF_3 favor an edge-inversion mechanism.[6,7] It has also been suggested that inversion at fluorine-substituted tertiary pnictine centers may proceed via a Y-shaped transition state (**III**), also of C_{2v} symmetry; however, subsequent calculations indicate that this is not a true transition state, but rather a second-order saddle point connecting two T-shaped structures.[8]

As part of an ongoing study into the chemistry of phosphatetrylenes $(R_2P)EX$ (E = Ge, Sn, Pb; X = e.g., halide, R_2P), we recently reported the synthesis and structural characterization of the heteroleptic compounds $[\{(Me_3Si)_2CH\}(C_6H_4\text{-}2\text{-}CH_2NMe_2)P]ECl$ [E = Ge (**1**), Sn (**2**)] and the homoleptic diphosphatetrylenes $[\{(Me_3Si)_2CH\}(C_6H_4\text{-}2\text{-}CH_2NMe_2)P]_2E$ [E = Ge (**3**), Sn (**4**)] (Chart 1).[9,10] These compounds possess pyramidal phosphorus and germanium/tin atoms and are thus chiral at each of these centers. Multielement and variable-temperature NMR studies have shown that compounds **1**−**4** are highly dynamic in solution due to the rapid interconversion of diastereomers via epimerization at either the phosphorus or germanium/tin centers.

Although it is not possible to distinguish between these epimerization processes experimentally, theoretical calculations provide a convenient method by which the barriers to inversion at the P and Ge/Sn centers may be investigated. Perhaps surprisingly, outside of our own preliminary studies, little is known about the inversion of pyramidal Ge(II) and Sn(II) species; such compounds are isoelectronic with the corresponding tertiary arsine and stibine, R_3As and R_3Sb, respectively. The absence of a comprehensive study of the inversion behavior of trigonal pyramidal germanium(II) or tin(II) compounds, coupled with the unusual conjunction of directly adjacent pyramidal Ge/Sn and P centers in **1**−**4**, both of which may undergo inversion, prompted us to consider these species in more detail; the results of this study are presented below.

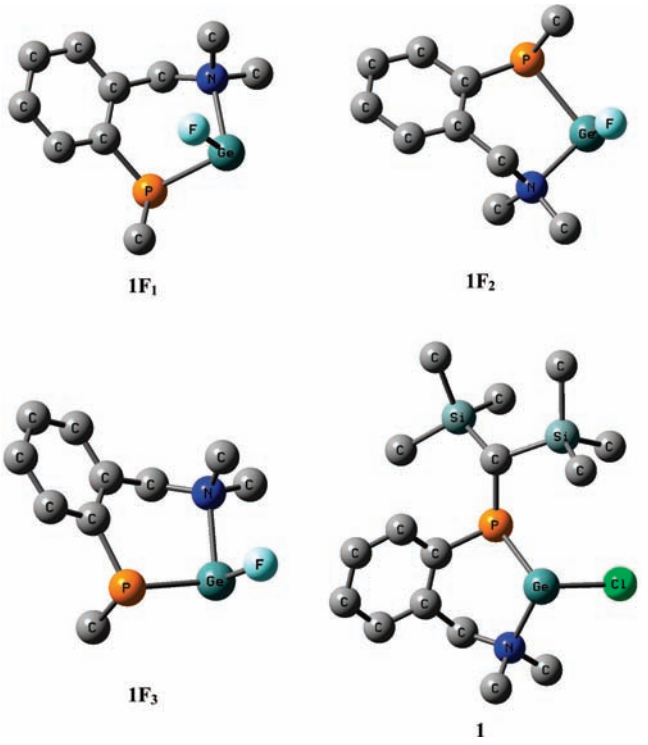

Figure 1. Optimized geometries for the local minima $\mathbf{1F_1}$, $\mathbf{1F_2}$, and $\mathbf{1F_3}$ [B3LYP/6-31G(d,p)] and the experimentally obtained crystal structure of **1** (H atoms omitted for clarity).

RESULTS AND DISCUSSION

Computational Details. Although our experimental data pertain to the sterically hindered phosphatetrylenes **1**−**4**,[9,10] these compounds are sufficiently large that a comprehensive theoretical treatment would be unfeasible. Therefore, in order to save on computational resources, we have confined the current study to the model phosphagermylenes $\{(Me)P(C_6H_4\text{-}2\text{-}CH_2NMe_2)\}GeX$ [X = F (**1F**), Cl (**1Cl**), Br (**1Br**), H (**1H**), Me (**1Me**)]. Our preliminary DFT studies have shown that ground state geometries obtained at the B3LYP/6-31G(d,p) level of theory for the closely related model compounds $\{(Me)P(C_6H_4\text{-}2\text{-}CH_2NMe_2)\}_2E$ (E = Ge, Sn) are very similar to the structures obtained by X-ray crystallography for **3** and **4**.[9,10] At this level of theory, bond lengths within the EP_2N cores are overestimated by approximately 0.02−0.10 Å in each case, a well-known defect of B3LYP calculations. However, there is a close correspondence between the calculated and experimental bond angles around the P and Ge centers. In addition, several previous studies have shown that calculations at the B3LYP/6-31G(d,p) level provide equilibrium geometries for related tertiary pnictine systems which correlate well with experiment; in these studies little advantage was found in using alternative correlated methods such as MP2, or more extended basis sets, for geometry optimizations.[2,7a] We

dx.doi.org/10.1021/ic200012v |*Inorg. Chem.* 2011, 50, 3651–3661

were, therefore, confident that optimizations performed on our model compounds at this level of theory would give representative geometries for these species.

Geometry optimizations of the ground state molecules were carried out at the B3LYP/6-31G(d,p) level of theory,[11,12] and stationary points were confirmed as local minima by the absence of negative vibrational frequencies. Transition states were initially located using the QST3 method[13] at the HF/3-21G* level of theory;[14] the geometries obtained were then reoptimized at the B3LYP/6-31G(d,p) level of theory and were confirmed as true transition states by the presence of a single negative vibrational frequency which correlated with the expected displacement vector for inversion at either phosphorus or germanium. It has been reported that the energies of systems containing "dative" covalent bonds (i.e., Lewis acid−base interactions) obtained using the B3LYP hybrid functional are not always accurate and that the effects of electron correlation are under-represented at this level of theory;[15] we have therefore obtained single-point energies for all ground and transition state geometries using the fully correlated MP2 method[16] both with the 6-31G(d,p) basis set and with the larger 6-311+G(2d,p) basis set,[17,18] which includes both polarization and diffuse functions. Further details of computational methods may be found in the Supporting Information.

Ground State Geometries. Three distinct local minima (**1X$_1$**, **1X$_2$**, and **1X$_3$**) were located for each of the molecules **1F**, **1Cl**, **1Br**, **1H**, and **1Me**. The optimized geometries of the representative conformations **1F$_1$**, **1F$_2$**, and **1F$_3$** are shown in Figure 1, and selected bond lengths and angles for all minimum energy geometries are given in Table 1; relative energies for all minima are given in Table 2. The ground state in each case (**1X$_1$**) consists of a trigonal pyramidal Ge center, coordinated by the P and N atoms of a chelating phosphide ligand and by the substituent X; the molecules are chiral at both the pyramidal Ge and P centers and have a Ge$_R$P$_S$ configuration. The angles about the germanium atoms lie close to 90° but show no obvious trends across the series; the rather small angles about Ge cause the substituent X to lie close to the aromatic ring in this conformation.

For **1F** the next highest energy conformation located in this study (**1F$_2$**) differs from the ground state largely in the orientation of the fluorine substituent, which lies in a position distal to the aromatic ring. At the MP2/6-31G(d,p)//B3LYP/6-31G(d,p) level of theory, this conformation lies just 15.4 kJ mol^{-1} higher in energy than the ground state. For the remaining model compounds this conformation represents the highest energy minimum located and lies between 18.4 and 22.2 kJ mol^{-1} higher in energy than the corresponding ground state geometry **1X$_1$**. The third minimum energy geometry located (**1X$_3$**) is the Ge$_R$P$_R$ epimer of **1X$_2$**. For all but **1F** this is the second lowest energy conformation; for **1F** this geometry lies 18.7 kJ mol^{-1} above the ground state, whereas for the remaining compounds this geometry lies between 9.6 and 21.8 kJ mol^{-1} higher in energy than the corresponding ground state geometry **1X$_1$**.

Table 2. Relative Energies of Local Minima 1X$_1$, 1X$_2$, and 1X$_3$ (kJ mol^{-1})

	B3LYP/6-31G(d,p)	MP2/6-31G(d,p)
1F$_1$	0.0	0.0
1F$_2$	11.4	15.4
1F$_3$	17.0	18.7
1Cl$_1$	0.0	0.0
1Cl$_2$	16.3	19.7
1Cl$_3$	11.7	13.8
1Br$_1$	0.0	0.0
1Br$_2$	16.3	22.2
1Br$_3$	14.6	21.8
1Me$_1$	0.0	0.0
1Me$_2$	17.2	20.5
1Me$_3$	8.0	13.0
1H$_1$	0.0	0.0
1H$_2$	16.3	18.4
1H$_3$	8.0	9.6

Table 1. Bond Lengths and Angles for the Local Minimum Geometries 1X$_1$, 1X$_2$, and 1X$_3$ and for the Crystallographically Characterized 1

	Ge−P (Å)	Ge−X (Å)	Ge−N (Å)	P−Ge−N (°)	N−Ge−X (°)	P−Ge−X (°)	ΣGe (°)[a]
1F$_1$	2.445	1.809	2.206	90.64	91.79	96.36	278.78
1F$_2$	2.468	1.825	2.169	95.08	86.85	97.79	279.73
1F$_3$	2.440	1.806	2.176	95.58	89.64	99.69	284.90
1Cl$_1$	2.444	2.311	2.261	87.57	98.14	99.35	285.06
1Cl$_2$	2.447	2.325	2.257	96.39	96.97	95.64	290.33
1Cl$_3$	2.422	2.316	2.158	93.26	94.41	98.51	286.18
1[b]	2.4205(16)	2.2965(16)	2.191(5)	88.70(13)	95.73(14)	99.42(6)	283.82
1Br$_1$	2.434	2.445	2.217	89.23	98.58	98.79	286.58
1Br$_2$	2.462	2.456	2.190	95.90	94.29	98.85	289.04
1Br$_3$	2.403	2.445	2.161	90.64	95.64	98.03	283.83
1Me$_1$	2.446	2.010	2.215	88.49	98.31	99.64	286.43
1Me$_2$	2.438	2.014	2.220	97.12	96.61	97.07	290.80
1Me$_3$	2.405	2.010	2.243	97.59	97.01	94.40	289.00
1H$_1$	2.430	1.597	2.175	90.73	89.32	92.24	272.29
1H$_2$	2.433	1.600	2.186	97.78	88.75	92.24	278.76
1H$_3$	2.392	1.591	2.204	98.17	88.91	89.75	275.83

[a] Sum of angles at the germanium center. [b] Experimentally determined values from X-ray crystallography.

dx.doi.org/10.1021/ic200012v |*Inorg. Chem.* 2011, 50, 3651–3661

The ground state geometry $\mathbf{1Cl_1}$ differs in conformation from the crystal structure of **1**, which adopts a Ge_RP_R conformation (for consistency we use the same Cahn−Ingold−Prelog priority for the $CH(SiMe_3)_2$ group in **1** as for the Me group in $\mathbf{1Cl_1}$). However, calculations on our model compounds are likely to underestimate the impact of steric effects associated with the bulky $CH(SiMe_3)_2$ group in **1**; in this regard, we note that all three minimum energy geometries lie close in energy and that the corresponding Ge_RP_R conformation $\mathbf{1Cl_3}$ lies just 13.8 kJ mol^{-1} higher in energy than the ground state. Although $\mathbf{1Cl_3}$ and **1** possess the same stereochemistry, the conformations of the chelate rings differ between these compounds, and this leads to small differences in their bond lengths and angles. The bond lengths within the GePNCl core of $\mathbf{1Cl_3}$ are close to those observed crystallographically for **1**;[10] for example, the Ge−P distances for $\mathbf{1Cl_3}$ and **1** are 2.422 and 2.4205(16) Å, respectively, while the Ge−Cl distances are 2.316 and 2.2965(16) Å, respectively. The calculated P−Ge−N angle for $\mathbf{1Cl_3}$ [93.26°] is somewhat larger than the corresponding angle in **1** [88.70(13)°], but there is a good correspondence between the P−Ge−Cl [98.51 and 99.42(6)°, respectively] and the N−Ge−Cl angles [94.41 and 95.73(14)°, respectively] in $\mathbf{1Cl_3}$ and **1**.

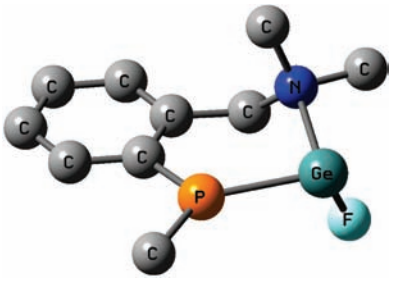

Figure 2. Transition state geometry $\mathbf{1F_4}$ [B3LYP/6-31G(d,p)] with H atoms omitted for clarity.

The relative energies of the higher energy local minima $\mathbf{1X_2}$ and $\mathbf{1X_3}$ are calculated to be slightly higher at the MP2/6-31G(d,p) compared to the B3LYP/6-31G(d,p) level of theory, although the relative ordering of these minima is the same for both methods. The reversal in the ordering of the higher energy conformations of $\mathbf{1F}$ ($\mathbf{1F_2} < \mathbf{1F_3}$) compared to the remaining structures ($\mathbf{1X_2} > \mathbf{1X_3}$, $X \neq F$) may reasonably be attributed to a steric effect. Pauling gives the van der Waals radii of F, Cl, Br, and Me as 1.35, 1.80, 1.95, and

Table 3. Bond Lengths (Å) and Angles (°) for the Ground and Transition States for Inversion at Phosphorus and Germanium in 1X

	Ge−P	Ge−X	Ge−N	P−C(Me)	P−C(Ar)	P−Ge−N	N−Ge−X	P−Ge−X	C1−P−C8	C1−P−Ge	C8−P−Ge	ΣP^a
$\mathbf{1F_1}$	2.445	1.809	2.206	1.877	1.843	90.64	91.79	96.36	101.93	93.68	96.10	291.71
$\mathbf{1F_4}$	2.373	1.819	2.181	1.850	1.794	86.25	85.55	101.77	112.20	127.89	119.91	360.00
$\mathbf{1F}^{Planar}_{N-F}$	2.289	1.809	2.815	1.849	1.816	75.81	165.24	89.80	109.45	116.59	130.86	356.90
$\mathbf{1F}^{Planar}_{P-F}$	2.627	1.833	2.315	1.866	1.811	79.94	85.21	164.31	105.27	131.73	123.00	360.00
$\mathbf{1F}^{Folded}_{N-F}$	2.409	1.800	2.822	1.871	1.863	75.70	163.48	96.45	103.59	100.58	82.76	286.92
$\mathbf{1F}^{Folded}_{P-F}$	—[b]	—	—	—	—	—	—	—	—	—	—	—
$\mathbf{1Cl_1}$	2.444	2.311	2.261	1.874	1.837	87.57	98.14	99.35	103.06	101.27	97.22	301.54
$\mathbf{1Cl_4}$	2.381	2.346	2.188	1.849	1.790	86.36	95.68	102.02	113.06	127.84	118.72	359.62
$\mathbf{1Cl}^{Planar}_{N-Cl}$	2.295	2.338	2.710	1.851	1.823	78.98	167.95	93.08	107.35	121.37	124.79	353.21
$\mathbf{1Cl}^{Planar}_{P-Cl}$	2.521	2.493	2.294	1.860	1.808	82.43	94.64	173.56	106.79	129.97	123.22	359.98
$\mathbf{1Cl}^{Folded}_{N-Cl}$	2.407	2.322	2.797	1.866	1.871	76.17	173.70	100.52	103.25	106.77	78.11	288.12
$\mathbf{1Cl}^{Folded}_{P-Cl}$	2.748	2.475	2.277	1.874	1.825	83.13	92.33	169.11	100.94	95.34	60.74	257.02
$\mathbf{1Br_1}$	2.434	2.445	2.217	1.871	1.840	89.23	98.58	98.79	103.13	97.52	97.01	297.66
$\mathbf{1Br_4}$	2.377	2.471	2.189	1.848	1.789	86.13	96.84	102.23	113.56	127.64	118.53	359.72
$\mathbf{1Br}^{Planar}_{N-Br}$	2.289	2.475	2.702	1.850	1.821	79.34	169.70	93.66	107.67	122.34	125.03	355.04
$\mathbf{1Br}^{Planar}_{P-Br}$	2.514	2.620	2.298	1.860	1.809	82.62	95.91	174.18	106.74	129.97	123.29	360.00
$\mathbf{1Br}^{Folded}_{N-Br}$	2.405	2.458	2.770	1.866	1.869	76.54	170.28	100.59	103.39	107.06	78.25	288.69
$\mathbf{1Br}^{Folded}_{P-Br}$	3.149	2.502	2.198	1.874	1.772	81.88	96.23	172.06	102.75	113.18	57.31	273.23
$\mathbf{1Me_1}$	2.446	2.010	2.215	1.874	1.838	88.49	98.31	99.64	102.91	98.96	97.06	298.93
$\mathbf{1Me_4}$	2.435	2.011	2.174	1.853	1.784	86.24	97.84	98.19	112.22	129.77	118.00	359.99
$\mathbf{1Me}^{Planar}_{N-Me}$	2.253	2.032	3.181	1.856	1.823	77.31	170.70	94.61	106.72	123.59	129.58	359.89
$\mathbf{1Me}^{Planar}_{P-Me}$	3.033	2.045	2.228	1.880	1.821	81.54	95.32	174.54	101.52	147.44	111.04	360.00
$\mathbf{1Me}^{Folded}_{N-Me}$	2.417	2.011	3.067	1.874	1.876	71.22	161.51	101.88	102.57	108.87	80.41	291.85
$\mathbf{1Me}^{Folded}_{P-Me}$	3.363	2.042	2.188	1.875	1.776	77.60	94.38	168.52	102.73	115.35	59.11	277.19
$\mathbf{1H_1}$	2.430	1.597	2.175	1.874	1.842	90.73	89.32	92.24	102.44	96.21	96.40	295.05
$\mathbf{1H_4}$	2.322	1.591	2.259	1.853	1.802	90.44	83.23	90.07	115.32	133.47	111.21	360.00
$\mathbf{1H_5}$	2.218	1.498	2.036	1.902	1.875	107.28	108.29	144.30	97.40	107.09	100.54	305.04
$\mathbf{1H}^{Planar}_{N-H}$	2.227	1.597	3.187	1.853	1.823	77.25	160.09	84.14	107.15	122.62	130.16	359.93
$\mathbf{1H}^{Planar}_{P-H}$	2.892	1.647	2.246	1.876	1.817	79.54	82.40	161.45	102.53	140.73	116.74	359.99
$\mathbf{1H}^{Folded}_{N-H}$	2.365	1.608	3.262	1.875	1.870	67.81	159.49	92.93	103.02	105.39	86.33	294.74
$\mathbf{1H}^{Folded}_{P-H}$	3.306	1.626	2.115	1.875	1.758	84.68	95.32	179.99	103.66	130.09	58.96	292.71

[a] Sum of angles at phosphorus. [b] Transition state not located (see text).

dx.doi.org/10.1021/ic200012v |*Inorg. Chem.* 2011, 50, 3651–3661

Table 4. Energies of Transition States $1X_4$ (Corresponding to Vertex-Inversion at Phosphorus) Relative to $1X_1$ in kJ mol^{-1}

	B3LYP/6-31G(d,p)	MP2/6-31G(d,p)	MP2/6-311+G(2d,p)
$1F_4$	69.3	78.3	66.1
$1Cl_4$	81.6	100.0	90.8
$1Br_4$	87.4	106.9	93.4
$1Me_4$	91.8	108.8	98.7
$1H_4$	87.4	96.0	83.5

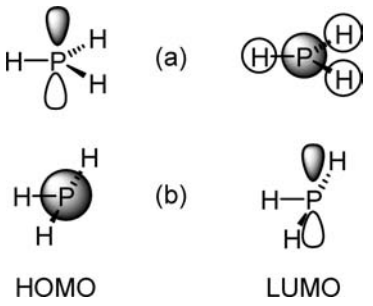

Figure 3. HOMO and LUMO of the transition states for (a) vertex- and (b) edge-inversion of PH_3.

2.00 Å, respectively;[19] the van der Waals radius of hydrogen is significantly affected by the electronegativity of the atom to which it is bound. While Bondi suggests a van der Waals radius of 1.20 Å for aliphatic hydrogen,[20] Batsanov suggests a value of 0.75 Å for the van der Waals radius of the hydrogen atom in HCl, but 1.52 Å in H_2;[21] since germanium is more electropositive than hydrogen, it is reasonable to assume that the van der Waals radius of the hydridic hydrogen in **1H** will exceed this latter value. In conformation $1X_2$ the substituent X lies in close proximity to the P-methyl and one of the N-methyl groups, whereas in $1X_3$ this substituent lies close to only one of the N-methyl groups and is therefore less sterically congested. Thus, steric repulsion between X and the P- and N-methyl groups in $1X_2$ is likely to be considerable for the larger substituents Cl, Br, H, and Me, outweighing any other stabilizing factors for this conformation over $1X_3$. Nonetheless, it is notable that the differences in energies between conformations $1X_2$ and $1X_3$ are only very small (lying between 0.4 and 8.8 kJ mol^{-1} at the MP2/6-31G(d,p) level of theory).

Inversion at Phosphorus. For all of the ground state conformations $1X_1$, a single transition state ($1X_4$) was located which corresponds to inversion at phosphorus. This contains a trigonal planar phosphorus atom and corresponds to a vertex-inversion process. We were unable to locate a transition state corresponding to edge-inversion at phosphorus for any of the model compounds; all such attempts converged to the vertex-inversion transition state $1X_4$. The geometry of transition state $1F_4$, which is representative of all the $1X_4$ geometries, is shown in Figure 2, and selected bond lengths and angles for all of the phosphorus inversion transition states $1X_4$ are given in Table 3; relative energies for transition states $1X_4$ are given in Table 4.

Previous calculations by Dixon and co-workers suggest that in the vertex-inversion transition state of PH_3 the lone pair on phosphorus lies in an out-of-plane p-type orbital of a_2'' symmetry (Figure 3).[6,7] Consistent with this, for all of the phosphorus inversion transition states $1X_4$ natural bond orbital (NBO) analyses[22] confirm that the lone pair on phosphorus is located in an orbital perpendicular to the C_2PGe plane of essentially pure 3p-character. This is clearly manifested in the P−Ge, P−C(Me), and P−C(Ar) distances, which decrease significantly on going from the pyramidal ground state conformation to the trigonal planar transition state, due to decreased repulsion between the phosphorus lone pair and the bonding electron pairs in the latter geometry.

Table 5. Wiberg Bond Indices for the Ground and Transition States for Inversion at Phosphorus and Germanium in 1X

	Ge−P	Ge−N	Ge−X	P−C(Ar)	P−C(Me)
$1F_1$	0.818	0.273	0.401	0.941	0.963
$1F_4$	0.851	0.285	0.376	1.019	0.988
$1F_{N-F}^{Planar}$	1.111	0.051	0.365	0.974	0.975
$1F_{P-F}^{Planar}$	0.774	0.231	0.296	0.969	0.958
$1F_{N-F}^{Folded}$	0.799	0.054	0.364	0.926	0.964
$1Cl_1$	0.849	0.276	0.661	0.944	0.965
$1Cl_4$	0.854	0.285	0.609	1.030	0.988
$1Cl_{N-Cl}^{Planar}$	1.149	0.070	0.604	0.967	0.976
$1Cl_{P-Cl}^{Planar}$	0.933	0.239	0.399	0.965	0.970
$1Cl_{N-Cl}^{Folded}$	0.826	0.060	0.622	0.911	0.965
$1Cl_{P-Cl}^{Folded}$	0.425	0.215	0.473	1.000	0.949
$1Br_1$	0.853	0.283	0.732	0.944	0.965
$1Br_4$	0.849	0.287	0.693	1.041	0.991
$1Br_{N-Br}^{Planar}$	1.173	0.070	0.678	0.967	0.976
$1Br_{P-Br}^{Planar}$	0.910	0.241	0.490	0.965	0.969
$1Br_{N-Br}^{Folded}$	0.826	0.063	0.708	0.911	0.965
$1Br_{P-Br}^{Folded}$	0.237	0.240	0.638	1.258	0.947
$1Me_1$	0.823	0.287	0.769	0.946	0.958
$1Me_4$	0.754	0.298	0.740	1.067	0.985
$1Me_{N-Me}^{Planar}$	1.218	0.022	0.732	0.970	0.958
$1Me_{P-Me}^{Planar}$	0.539	0.236	0.548	1.015	0.933
$1Me_{N-Me}^{Folded}$	0.817	0.030	0.712	0.913	0.949
$1Me_{P-Me}^{Folded}$	0.256	0.243	0.603	1.222	0.941
$1H_1$	0.845	0.305	0.896	0.940	0.958
$1H_4$	0.944	0.255	0.883	0.974	0.982
$1H_5$	1.136	0.398	0.963	0.884	0.879
$1H_{N-H}^{Planar}$	1.317	0.019	0.853	0.956	0.956
$1H_{P-H}^{Planar}$	0.638	0.257	0.734	0.992	0.941
$1H_{N-H}^{Folded}$	0.874	0.018	0.858	0.917	0.950
$1H_{P-H}^{Folded}$	0.129	0.297	0.842	1.434	0.943

For a trigonal pyramidal PnR_3 molecule, the barrier to vertex-inversion is a function of the difference in energy between the $2a_1$ HOMO in the ground state C_{3v} geometry and the a_2'' HOMO in the D_{3h} transition state.[23] The ground state $2a_1$ orbital is stabilized by mixing with the $3a_1$ LUMO (a second-order Jahn−Teller effect); greater mixing is possible when the HOMO−LUMO gap is small, lowering the energy of the $2a_1$ HOMO in the ground state and so increasing the barrier to inversion. The presence of electropositive substituents causes all of the orbitals in both the ground and transition states to increase in energy, especially those with high coefficients at the substituents. However, the a_2'' HOMO in the D_{3h} transition state is nonbonding and is located on the central atom and so is only slightly raised in energy. Therefore, the energy difference between the ground and transition state HOMOs is reduced and so the barrier to inversion is decreased.

Somewhat surprisingly however, we find that the relative barriers to inversion at phosphorus via transition states $1X_4$

dx.doi.org/10.1021/ic200012v |Inorg. Chem. 2011, 50, 3651–3661

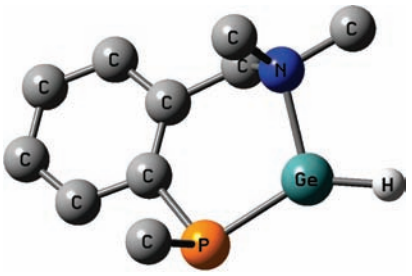

Figure 4. Optimized geometry of transition state $\mathbf{1H_5}$ [B3LYP/6-31G(d,p)] with H atoms, other than that bound to Ge, omitted for clarity.

increase in the order $\mathbf{1F_4} < \mathbf{1Cl_4} < \mathbf{1Br_4} < \mathbf{1Me_4}$, i.e., with *decreasing* electronegativity of the substituent X (the Pauling electronegativities for F, Cl, Br, and Me are 3.98, 3.16, 2.96, 2.52, respectively).[19] This behavior cannot be explained using the arguments presented above, since an electronegative substituent X would be expected to make the adjacent germanium center more electron poor and so stabilize all orbitals except the transition state HOMO, leading to an increase in the barrier to inversion. Rather, we tentatively suggest that these transition states are stabilized by delocalization of the phosphorus lone pair; the presence of electronegative substituents at germanium enhances this delocalization, stabilizing the transition state and so lowering the barrier to inversion. Although such an interaction is likely not to be completely responsible for the increased stabilization of these transition states with increasing electronegativity of the substituent X, NBO analyses reveal significant delocalization of the phosphorus lone pair into both a π-antibonding orbital of the aromatic ring and a vacant Ge−X σ^* orbital. For these four transition states, the latter interaction is greatest for $\mathbf{1F_4}$ and $\mathbf{1Cl_4}$ (with $E(2)$ energies of 124.9 and 164.8 kJ mol^{-1}, respectively) and lowest for $\mathbf{1Me_4}$ (with an $E(2)$ energy of just 23.4 kJ mol^{-1}). Consistent with this, for these four compounds the Wiberg bond indices (WBIs) for the P−C(Ar) bond are significantly higher in transition states $\mathbf{1X_4}$ than in the corresponding ground states (Table 5).

Although the Pauling electronegativity of H is 2.20, the relative energy of $\mathbf{1H_4}$ lies between those of $\mathbf{1F_4}$ and $\mathbf{1Cl_4}$ at the MP2/6-311+G(2d,p)//B3LYP/6-31G(d,p) level of theory. It is difficult to account for the anomalous vertex-inversion barrier for $\mathbf{1H_4}$, although it may be a consequence of the highly polarizable nature of the electron density associated with the hydridic hydrogen atom. It is notable that for this transition state the $E(2)$ energy for the delocalization of the phosphorus lone pair onto germanium (65.3 kJ mol^{-1}) is substantially greater than for $\mathbf{1Me_4}$.

Inversion at Germanium. A transition state corresponding to vertex-inversion at the germanium center was located only for **1H**; all attempts to locate a transition state of this nature for the remaining compounds yielded geometries corresponding to edge-inversion at germanium. This is consistent with previous observations that electronegative substituents favor edge- over vertex-inversion (see above). The optimized geometry of this transition state ($\mathbf{1H_5}$) is shown in Figure 4, and selected bond lengths and angles are given in Table 3; relative energies are given in Table 6.

Transition state $\mathbf{1H_5}$ possesses an essentially planar germanium center, while the phosphorus center retains a pyramidal geometry (sum of angles at germanium 359.87°; sum of angles at phosphorus 305.04°). The P−Ge−N bite angle of the phosphide ligand is significantly wider in $\mathbf{1H_5}$ than in the ground state geometry (107.28 vs 90.73°), while the Ge−N, Ge−P, and Ge−H distances are all substantially shorter in $\mathbf{1H_5}$ than in $\mathbf{1H_1}$, consistent with localization of the germanium lone pair in a p-orbital perpendicular to the GePNH plane; NBO analysis indicates that the germanium lone pair in this transition state has 99.94% 4p$_z$-character. Inversion via this mechanism is substantially disfavored: the barrier to inversion via transition state $\mathbf{1H_5}$ is calculated to be 221.6 kJ mol^{-1}.

Table 6. Energies of Transition States Involving Inversion at Germanium Relative to the Ground States $\mathbf{1X_1}$ (kJ mol^{-1})

	B3LYP/6-31G(d,p)	MP2/6-31G(d,p)	MP2/6-311+G(2d,p)
$\mathbf{1F}^{\text{Planar}}_{\text{N−F}}$	93.4	116.5	94.1
$\mathbf{1F}^{\text{Planar}}_{\text{P−F}}$	172.8	197.2	169.3
$\mathbf{1F}^{\text{Folded}}_{\text{N−F}}$	73.3	90.9	76.9
$\mathbf{1F}^{\text{Folded}}_{\text{P−F}}$	—[a]	—	—
$\mathbf{1Cl}^{\text{Planar}}_{\text{N−Cl}}$	89.9	116.6	100.3
$\mathbf{1Cl}^{\text{Planar}}_{\text{P−Cl}}$	176.3	216.0	186.7
$\mathbf{1Cl}^{\text{Folded}}_{\text{N−Cl}}$	72.8	92.7	82.7
$\mathbf{1Cl}^{\text{Folded}}_{\text{P−Cl}}$	150.0	154.9	146.9
$\mathbf{1Br}^{\text{Planar}}_{\text{N−Br}}$	97.4	129.3	101.8
$\mathbf{1Br}^{\text{Planar}}_{\text{P−Br}}$	184.2	222.2	185.4
$\mathbf{1Br}^{\text{Folded}}_{\text{N−Br}}$	79.6	104.7	85.5
$\mathbf{1Br}^{\text{Folded}}_{\text{P−Br}}$	157.6	171.6	156.1
$\mathbf{1Me}^{\text{Planar}}_{\text{N−Me}}$	106.8	143.2	109.0
$\mathbf{1Me}^{\text{Planar}}_{\text{P−Me}}$	251.8	306.5	264.3
$\mathbf{1Me}^{\text{Folded}}_{\text{N−Me}}$	99.0	125.3	103.1
$\mathbf{1Me}^{\text{Folded}}_{\text{P−Me}}$	195.6	219.0	196.1
$\mathbf{1H_5}$	233.1	224.3	221.6
$\mathbf{1H}^{\text{Planar}}_{\text{N−H}}$	100.1	128.8	97.1
$\mathbf{1H}^{\text{Planar}}_{\text{P−H}}$	252.3	294.7	257.7
$\mathbf{1H}^{\text{Folded}}_{\text{N−H}}$	109.1	133.8	107.1
$\mathbf{1H}^{\text{Folded}}_{\text{P−H}}$	204.2	218.7	208.4

[a] Transition state not located (see text).

For all but **1F**, four distinct transition states were located which correspond to edge-inversion at germanium. Due to the asymmetric nature of the chelating phosphide ligand, two T-shaped arrangements are possible: either the phosphorus center lies in an equatorial position with the N and X centers in trans-axial positions ($\mathbf{1X_{N−X}}$), or else the nitrogen center lies in an equatorial position with the P and X centers in trans-axial positions ($\mathbf{1X_{P−X}}$) (Figure 5).

For each of these arrangements, two distinct transition states were located. Our initial calculations located a rather unusual transition state in which both the germanium and phosphorus centers approach planarity ($\mathbf{1X}^{\text{Planar}}_{\text{N−X}}$ and $\mathbf{1X}^{\text{Planar}}_{\text{P−X}}$). We subsequently located a second pair of transition states, for all compounds except **1F**, in which only the germanium center is planar, but in which the aromatic ring is significantly folded toward the germanium atom ($\mathbf{1X}^{\text{Folded}}_{\text{N−X}}$ and $\mathbf{1X}^{\text{Folded}}_{\text{P−X}}$); we were unable to locate a stable transition state corresponding to $\mathbf{1F}^{\text{Folded}}_{\text{P−F}}$. Representative geometries are shown in Figure 6, selected bond lengths and angles are given in Table 3, and relative energies are given in Table 6.

In transition states $\mathbf{1X}^{\text{Planar}}_{\text{N−X}}$ the phosphorus center adopts a trigonal planar geometry, while the germanium center adopts a T-shaped geometry in which the N and X atoms are mutually trans. The lone pair at the germanium center has largely 4s-character, as expected, while the lone pair at phosphorus is essentially an

dx.doi.org/10.1021/ic200012v |*Inorg. Chem.* 2011, 50, 3651–3661

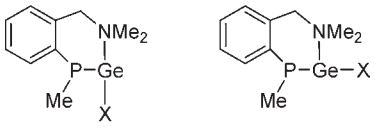

$\mathbf{1X}_{N\text{-}X}$ $\mathbf{1X}_{P\text{-}X}$

Figure 5. The two possible ligand arrangements in the edge-inversion transition states of **1X**.

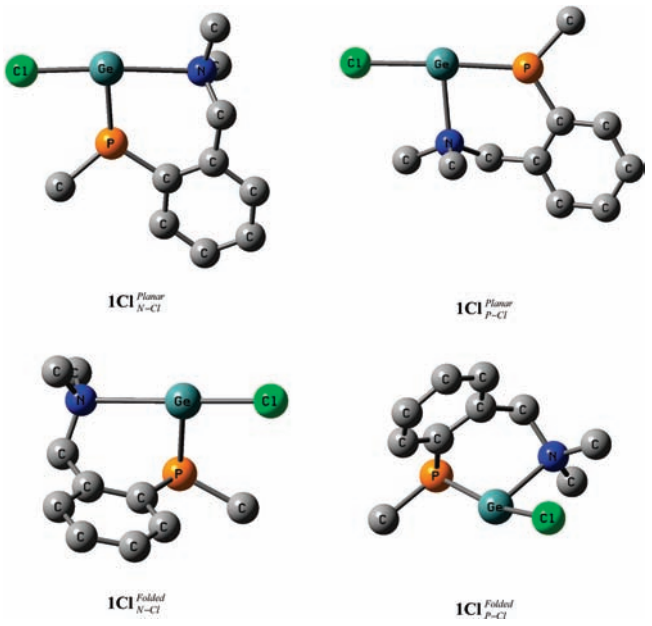

Figure 6. Transition state geometries for edge-inversion at germanium in **1Cl** [B3LYP/6-31G(d,p)] with H atoms omitted for clarity.

sp^3-hybrid in $\mathbf{1F}^{Planar}_{N-F}$, $\mathbf{1Cl}^{Planar}_{N-Cl}$, and $\mathbf{1Br}^{Planar}_{N-Br}$ but has effectively pure 3p-character in $\mathbf{1Me}^{Planar}_{N-Me}$ and $\mathbf{1H}^{Planar}_{N-H}$. In all of these transition states the formally vacant orbital at germanium has essentially 100% 4p-character.

In such a T-shaped transition state, the bonds between the axial substituents and the central germanium atom arise from a three-center–four-electron hypervalent bonding interaction, in which each of the Ge–X and Ge–N bonds has a formal bond order of 0.5, and in which the nonbonding orbital is primarily localized on the X and N atoms. This is clearly reflected in the very long Ge–N distances: for $\mathbf{1F}^{Planar}_{N-F}$, $\mathbf{1Cl}^{Planar}_{N-Cl}$, and $\mathbf{1Br}^{Planar}_{N-Br}$, these distances are 0.609, 0.449, and 0.485 Å, respectively, greater than the Ge–N distances in the corresponding ground states. In these transition states the coefficient of the hypervalent nonbonding orbital will be largest at the electronegative nitrogen and halogen atoms, stabilizing this interaction. However, in $\mathbf{1Me}^{Planar}_{N-Me}$ and $\mathbf{1H}^{Planar}_{N-H}$ the more electropositive Me or H substituent is less able to support this nonbonding electron density and so the coefficient of this orbital at the methyl or hydride substituent is reduced and the coefficient at nitrogen is increased; the nonbonding orbital thus becomes essentially antibonding with respect to the Ge and N atoms and bonding with respect to the Ge–H/Me atoms, i.e., the Ge–N bond order tends to zero, while the Ge–H/Me bond tends to a straightforward σ-bond. This is reflected in the Ge–N and Ge–X distances in these transition states: in $\mathbf{1Me}^{Planar}_{N-Me}$ the Ge–N distance is 0.966 Å longer than in the ground state, whereas the Ge–C distance is just 0.021 Å longer than in $\mathbf{1Me_1}$. In $\mathbf{1H}^{Planar}_{N-H}$ the Ge–N distance is 1.012 Å longer than in the ground state, whereas the Ge–H distances in this transition state and in the ground state are identical. Consistent with this, the WBIs for the Ge–N bonds in $\mathbf{1X}^{Planar}_{N-X}$ are substantially lower than in the ground state; for example, the WBIs for $\mathbf{1F_1}$ and $\mathbf{1F}^{Planar}_{N-F}$ are 0.273 and 0.051, respectively.

For $\mathbf{1F}^{Planar}_{N-F}$, $\mathbf{1Cl}^{Planar}_{N-Cl}$, and $\mathbf{1Br}^{Planar}_{N-Br}$, the Ge–X distances are 0.000, 0.027, and 0.030 Å greater, respectively, than the Ge–X distances in the corresponding ground states. However, for these transition states a somewhat different explanation may prevail. In contrast to $\mathbf{1Me}^{Planar}_{N-Me}$ and $\mathbf{1H}^{Planar}_{N-H}$, the electronegative halogen atoms are able to support a significant proportion of the hypervalent nonbonding electron density, and so the σ-bonding situation for the axial substituents is close to a typical three-center–four-electron interaction. The small difference in Ge–X bond lengths between $\mathbf{1X_1}$ and $\mathbf{1X}^{Planar}_{N-X}$ may be attributed to complementary pπ–pπ bonding between the vacant p-orbital on germanium and one of the lone pairs on the halogen atom, counteracting the bond lengthening effect of the hypervalent σ-bonding situation for these atoms. Inspection of the molecular orbitals reveals low-lying Ge–X π-interactions; for example, the highest energy molecular orbitals exhibiting significant Ge–F and Ge–Cl π-interactions are the HOMO–10 and HOMO–6, respectively. In this regard, it is notable that the Ge–X WBIs are very similar in $\mathbf{1X}^{Planar}_{N-X}$ and the corresponding ground states $\mathbf{1X_1}$.

The Ge–P distances in these transition states are significantly shorter than the Ge–P distances in the corresponding ground states, consistent with a typical σ-bond supplemented by significant pπ–pπ interactions between the p-type lone pair at phosphorus and the vacant p_z-orbital at germanium. For each of these transition states, inspection of the molecular orbitals reveals that the HOMO comprises a π-type orbital localized largely on the Ge and P atoms. This is reflected in the WBIs for these interactions, which are substantially higher in the transition states than in the corresponding ground states (see Table 5).

For transition states $\mathbf{1X}^{Planar}_{P-X}$, a similar situation arises: the phosphorus and germanium centers adopt trigonal planar and T-shaped geometries, respectively. The lone pair and vacant p-orbitals at germanium have essentially pure 4s- and pure $4p_z$-character, respectively; perhaps surprisingly, the lone pair at phosphorus has between 61.5 and 68.1% 3s-character. Once again the bonds between germanium and the axial substituents are longer than the corresponding distances in the respective ground states; this lengthening is most pronounced for the Ge–P distances in $\mathbf{1Me}^{Planar}_{P-Me}$ and $\mathbf{1H}^{Planar}_{P-H}$ and has the same origins as the increased bond lengthening for the Ge–N distances in $\mathbf{1Me}^{Planar}_{N-Me}$ and $\mathbf{1H}^{Planar}_{N-H}$. Inspection of the molecular orbitals reveals low-lying orbitals corresponding to Ge–X π-interactions for $\mathbf{1F}^{Planar}_{P-F}$, $\mathbf{1Cl}^{Planar}_{P-Cl}$, and $\mathbf{1Br}^{Planar}_{P-Br}$ and, for all transition states $\mathbf{1X}^{Planar}_{P-X}$, a HOMO comprised largely of a Ge–P π-type orbital. The bonds between germanium and the equatorial N-substituent are also longer in these transition states than in the corresponding ground states. This contrasts with the observation by Dixon and Arduengo and others that the P–F_{eq} bond in the edge-inversion transition state of PF_3 is shorter than the P–F distance in the ground state.[6] However, this difference may readily be attributed to the ability of fluorine to participate in pπ–pπ interactions in the latter transition state, compared to the nitrogen in $\mathbf{1X}^{Planar}_{P-X}$, which may only form a dative Ge–N σ-bond; thus, the nitrogen atom experiences repulsion from the s-type lone pair at germanium, which cannot be mitigated by pπ–pπ interactions.

dx.doi.org/10.1021/ic200012v |*Inorg. Chem.* 2011, 50, 3651–3661

Table 7. Distances (Å) between Germanium and the *ipso*-Carbon Atoms in Transition States $1X_{N-X}^{Folded}$ and $1X_{P-X}^{Folded}$ with Distances for the Corresponding Ground States $1X_1$ Included for Comparison (Wiberg Bond Indices in Square Brackets)

	Ge...$C_{ipso}(CH_2)$ (Å)			Ge...C_{ipso}(P) (Å)			Ge−P−C_{ipso} (°)		
X	$1X_1$	$1X_{N-X}^{Folded}$	$1X_{P-X}^{Folded}$	$1X_1$	$1X_{N-X}^{Folded}$	$1X_{P-X}^{Folded}$	$1X_1$	$1X_{N-X}^{Folded}$	$1X_{P-X}^{Folded}$
F	3.499	3.417	–	3.215	2.854	–	96.10	82.76	–
	[0.009]	[0.014]	[–]	[0.015]	[0.046]	[–]			
Cl	3.541	3.313	2.712	3.236	2.727	2.444	97.22	78.11	60.74
	[0.011]	[0.021]	[0.083]	[0.016]	[0.075]	[0.119]			
Br	3.505	3.301	2.333	3.225	2.729	2.651	97.01	78.25	57.31
	[0.010]	[0.021]	[0.267]	[0.017]	[0.074]	[0.060]			
Me	3.500	3.483	2.557	3.235	2.802	2.887	97.06	80.41	59.11
	[0.010]	[0.020]	[0.207]	[0.019]	[0.066]	[0.027]			
H	3.471	3.660	2.210	3.209	2.920	2.833	96.40	86.33	58.96
	[0.010]	[0.011]	[0.426]	[0.018]	[0.049]	[0.029]			

In transition states $1X_{N-X}^{Folded}$, only the germanium centers adopt a planar (T-shaped) geometry, while the phosphorus atoms remain pyramidal. As observed for transition states $1X_{N-X}^{Planar}$, the Ge−P distances are somewhat shorter in $1X_{N-X}^{Folded}$ than in the corresponding ground states; however, this bond shortening is substantially less pronounced in the latter transition state due to the absence of significant P−Ge pπ−pπ interactions. Similarly, the Ge−N distances are substantially longer in $1X_{N-X}^{Folded}$ than in the corresponding ground state geometries.

Perhaps the most unusual aspect of transition states $1X_{N-X}^{Folded}$ is that in each case the aromatic ring of the phosphide ligand is folded over such that there is a relatively close contact between the germanium atom and the *ipso*-carbon of the ring directly bonded to phosphorus (Table 7).

In $1X_{P-X}^{Folded}$ the phosphorus atoms once again adopt a trigonal pyramidal geometry. As observed in $1X_{N-X}^{Folded}$, the aromatic ring in each case is folded toward the germanium center; however, in $1X_{P-X}^{Folded}$ there is a close contact between the germanium atom and the *ipso*-carbon directly bonded to the dimethylaminomethyl group (Table 7). The folding in transition states $1X_{P-X}^{Folded}$ appears to be more pronounced than in $1X_{N-X}^{Folded}$, significantly affecting the bonding in the aromatic ring such that the following occur: (i) the benzylic carbon atom deviates significantly from coplanarity with the aromatic ring, (ii) the C−C_{ipso} distances within the ring increase substantially (by up to 0.09 Å) compared to the corresponding distances in the ground state geometries, and (iii) the rings themselves distort appreciably from planarity.

The greatest effect is observed in $1Br_{P-Br}^{Folded}$ and $1H_{P-H}^{Folded}$, where the *ipso*-carbon bonded to the dimethylaminomethyl group is significantly distorted away from planarity. Indeed, for these two transition states, NBO analyses suggest a substantial bonding interaction between the germanium and *ipso*-carbon atoms, with concomitant dearomatization of the ring; this is consistent with the short Ge...$C_{ipso}(CH_2)$ distances and the extremely long Ge−P distances in these cases (the Ge−P distances for $1Br_{P-Br}^{Folded}$ and $1H_{P-H}^{Folded}$ are 3.149 and 3.306 Å, respectively). The P−C(Ar) distances in $1Br_{P-Br}^{Folded}$ and $1H_{P-H}^{Folded}$ are also substantially shorter (1.772 and 1.758 Å, respectively) than in the corresponding ground states (1.840 and 1.842 Å, respectively), consistent with the development of P−C(Ar) multiple-bond character associated with dearomatization of the ring. Supporting this, the WBIs for the Ge...$C_{ipso}(CH_2)$ interactions are 0.267 and 0.426 for $1Br_{P-Br}^{Folded}$ and $1H_{P-H}^{Folded}$, respectively, compared with a WBI of 0.010 for this interaction in both ground states. Similarly, the WBIs for the P−C(Ar) bond increase from 0.944 and 0.940 in $1Br_1$ and $1H_1$, respectively, to 1.258 and 1.434 in $1Br_{P-Br}^{Folded}$ and $1H_{P-H}^{Folded}$, respectively.

Scheme 2. (a) Stabilization of T-Shaped Transition States PnABC through Intra- or Intermolecular Donation of Lone Pairs into the Vacant Pnictogen p_z-Orbital (Pn = P, AS, Sb, Bi); (b) Stabilization through Intramolecular Donation of π-Electron Density in $1X_{N-X}^{Folded}$ (Left) and $1X_{P-X}^{Folded}$ (Right)

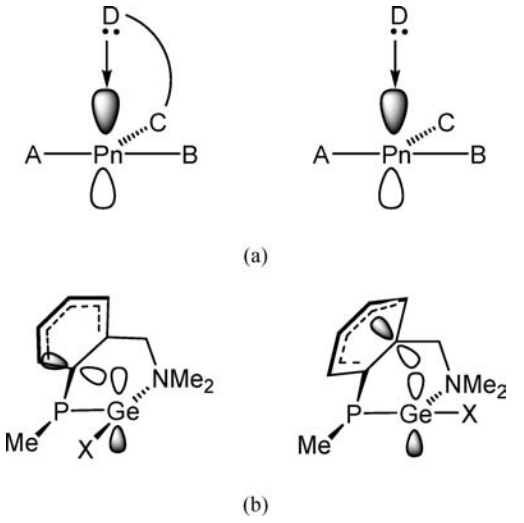

The above suggests that transition states $1X_{N-X}^{Folded}$ and $1X_{P-X}^{Folded}$ are stabilized by delocalization of electron density from the π-system of the aromatic ring into the vacant p_z-orbital at germanium. This is clearly related to the observation by Arduengo and co-workers and by Akiba and co-workers that edge-inversion of tertiary pnictines is accelerated significantly in the presence of intramolecularly coordinating donor groups or donor solvents such as pyridine.[24,25] In such cases the T-shaped transition state is stabilized by the intra- or intermolecular donation of lone pair(s) into the vacant p_z-orbital at the pnictogen atom (Scheme 2a). For $1X_{N-X}^{Folded}$ and $1X_{P-X}^{Folded}$, the function of the donor group is filled by the π-system of the aromatic ring of the phosphide ligand, which donates electron density into the vacant p_z-orbital at germanium, stabilizing these transition states (Scheme 2b); we term this new inversion pathway "aromatic anchimerically assisted edge-inversion".

dx.doi.org/10.1021/ic200012v |*Inorg. Chem.* 2011, 50, 3651–3661

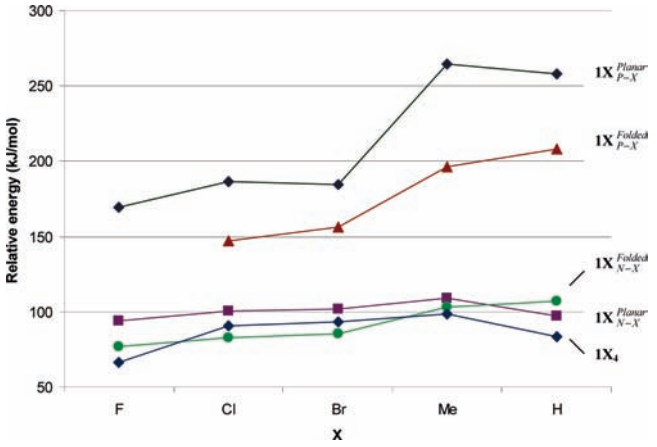

Figure 7. Energies (in kJ mol^{-1}) of transition states relative to the ground states $\mathbf{1X_1}$.

Relative Barriers to Inversion. The trends in barrier height for inversion at phosphorus (via transition states $\mathbf{1X_4}$) are described above and may largely be related to the electronegativity of the substituents, which enhance delocalization of the phosphorus lone pair in the transition states. In general, a similar relationship is observed for inversion at germanium: for each of the series of transition states $\mathbf{1X}^{\text{Planar}}_{\text{P}-\text{X}}$, $\mathbf{1X}^{\text{Folded}}_{\text{P}-\text{X}}$, and $\mathbf{1X}^{\text{Folded}}_{\text{N}-\text{X}}$, there is a gradual increase in the barrier to inversion at germanium with decreasing electronegativity of the substituent X, as expected for such edge-inversion processes (Figure 7). For both $\mathbf{1X}^{\text{Planar}}_{\text{P}-\text{X}}$ and $\mathbf{1X}^{\text{Folded}}_{\text{P}-\text{X}}$, there is a marked increase in this barrier when the substituent is either Me or H, both of which are unable either to participate in stabilizing $p\pi-p\pi$ interactions with the vacant p_z-orbital at germanium or to stabilize the hypervalent σ-bonding situation for the axial groups in these transition states (see above); for the remaining transition states this dramatic increase in barrier height is not observed. The trend in barrier heights for transition states $\mathbf{1X}^{\text{Planar}}_{\text{N}-\text{X}}$ appears somewhat anomalous; indeed, for this series the second lowest barrier to inversion, after that of $\mathbf{1F}^{\text{Planar}}_{\text{N}-\text{F}}$ (94.1 kJ mol^{-1}), is calculated for $\mathbf{1H}^{\text{Planar}}_{\text{N}-\text{H}}$ (97.1 kJ mol^{-1}), although the range of barrier heights for this transition state is rather small (94.1−109.0 kJ mol^{-1}). In fact, barriers to inversion via both $\mathbf{1X}^{\text{Planar}}_{\text{N}-\text{X}}$ and $\mathbf{1X}^{\text{Folded}}_{\text{N}-\text{X}}$ vary relatively little across the series (for $\mathbf{1X}^{\text{Folded}}_{\text{N}-\text{X}}$ the barrier heights fall in the range 76.9−107.1 kJ mol^{-1}).

Transition states $\mathbf{1X}^{\text{Planar}}_{\text{N}-\text{X}}$ and $\mathbf{1X}^{\text{Planar}}_{\text{P}-\text{X}}$ correspond to a cooperative process involving both edge-inversion at germanium and vertex-inversion at phosphorus and, as such, might be expected to have the highest barriers to inversion. However, the concomitant inversion at phosphorus appears not to be the defining factor in determining the relative barrier to inversion at germanium. Thus, whereas transition states $\mathbf{1X}^{\text{Planar}}_{\text{P}-\text{X}}$ are the highest energy transition states located for each substituent X, with relative energies ranging from 169.3 to 264.3 kJ mol^{-1}, transition states $\mathbf{1X}^{\text{Planar}}_{\text{N}-\text{X}}$ are substantially lower in energy, with relative energies ranging from 94.1 to 109.0 kJ mol^{-1}; indeed, $\mathbf{1H}^{\text{Planar}}_{\text{N}-\text{H}}$ is only the second highest energy transition state located for **1H** and, for this compound, has a higher barrier to inversion than only $\mathbf{1H_4}$ (which corresponds to inversion solely at the phosphorus center). Transition states $\mathbf{1X}^{\text{Folded}}_{\text{P}-\text{X}}$ form the second highest energy series of transition states for each substituent X (with barrier heights ranging from 146.9 to 208.4 kJ mol^{-1}), whereas $\mathbf{1X}^{\text{Folded}}_{\text{N}-\text{X}}$ have barriers to inversion similar to those for inversion via transition states $\mathbf{1X}^{\text{Planar}}_{\text{N}-\text{X}}$ and $\mathbf{1X_4}$. This clearly implies that the dominant factor in determining the barrier to edge-inversion at germanium is the nature of the groups in the axial positions. The T-shaped transition states are significantly stabilized by the presence of electronegative substituents in the hypervalently bonded axial positions, which are better able to support the substituent-centered nonbonding component, whether these can participate in $p\pi-p\pi$ interactions or not. Thus, T-shaped transition states where nitrogen adopts an axial position are substantially more stable than those where phosphorus lies in an axial position. Indeed, the ability of the phosphorus or X substituent to participate in $p\pi-p\pi$ bonding interactions with the vacant p_z-orbital at germanium appears to be only a secondary consideration, although we note here that all of the edge-inversion transition states located for **1F**, **1Cl**, and **1Br** benefit to at least some extent from stabilizing Ge−X $p\pi-p\pi$ interactions. In addition, in view of the similar energies for transition states $\mathbf{1X}^{\text{Planar}}_{\text{N}-\text{X}}$ and $\mathbf{1X}^{\text{Folded}}_{\text{N}-\text{X}}$, it appears that delocalization of electron density from either a planar phosphorus center or the aromatic ring of the ligand stabilizes the T-shaped transition states to a very similar extent.

CONCLUSIONS

The current study represents the first in-depth investigation of the inversion behavior of trigonal pyramidal germanium(II) compounds. While in many respects this parallels the behavior of the isoelectronic tertiary pnictines, this study reveals some quite intriguing features. In particular, the juxtaposition of the pyramidal Ge and P centers, each of which is able to undergo inversion, directly adjacent to one another provides a means to deconvolute the relative influence of σ-withdrawing and π-donating effects on the stability of the respective transition states. The most important findings from the present study are summarized below:

(i) Interconversion between stereoisomers of **1X** may occur via several mechanisms involving inversion solely at phosphorus, solely at germanium, or, simultaneously at phosphorus and germanium. The latter mechanism interconverts two enantiomers, whereas the first two inversion mechanisms result in epimerization of **1X**.

(ii) Inversion solely at phosphorus proceeds via a vertex-inversion mechanism in each case; the barrier to inversion decreases with increasing electronegativity of the substituent X due to increasing delocalization of the p-type phosphorus lone pair in the transition state.

(iii) Inversion at germanium via a vertex-inversion mechanism is observed only for **1H** and is highly disfavored; this is consistent with previous observations that the inversion of tertiary pnictines PnX_3 via this mechanism is disfavored when X is an electronegative substituent.

(iv) In all cases inversion at germanium via a T-shaped (edge-inversion) transition state is favored; for all bar **1H**, attempts to locate transition states corresponding to vertex-inversion converged to T-shaped geometries. For each arrangement of the substituents (P trans to X or N trans to X), two distinct transition states may be located, $\mathbf{1X}^{\text{Planar}}$ and $\mathbf{1X}^{\text{Folded}}$. In the former, inversion at germanium via a T-shaped geometry is accompanied by inversion at phosphorus via a trigonal planar geometry, whereas in the latter, inversion occurs solely at the germanium center and is accompanied by a folding of the ligand such that the aromatic ring lies in close proximity to the germanium center.

dx.doi.org/10.1021/ic200012v |*Inorg. Chem.* 2011, 50, 3651–3661

(v) In transition states $\mathbf{1X}^{\mathrm{Planar}}$, the germanium center is stabilized by π-donation from the phosphorus lone pair into the vacant p_z-orbital at germanium; for **1F**, **1Cl**, and **1Br** there is additional stabilization through $p\pi-p\pi$ interactions with the halogen lone pairs. Transition states $\mathbf{1X}^{\mathrm{Folded}}$ are stabilized by donation of electron density from the aromatic ring into the vacant p-orbital at germanium. Such an "aromatic anchimerchically assisted" inversion process has not been observed previously; its location suggests that the inversion mechanisms of trigonal pyramidal main group compounds may be much more complicated than previously thought, especially where compounds have aromatic or unsaturated substituents or where aromatic solvents are employed. The interaction between the aromatic ring and the germanium center appears to be significant, resulting in dearomatization of the ring and incipient $Ge-C_{ipso}$ bond formation in some cases.

(vi) The two possible arrangements of the substituents permit us to distinguish unambiguously between the effects of σ-withdrawing and π-donating groups on the stabilities of edge-inversion transition states. From the data presented above, it is quite clear that stabilization of these transition states is dominated by the presence of σ-withdrawing substituents in the axial positions. Thus, transition states $\mathbf{1X}^{\mathrm{Planar}}_{\mathrm{N-X}}$ and $\mathbf{1X}^{\mathrm{Folded}}_{\mathrm{N-X}}$ are significantly more stable than transition states $\mathbf{1X}^{\mathrm{Planar}}_{\mathrm{P-X}}$ and $\mathbf{1X}^{\mathrm{Folded}}_{\mathrm{P-X}}$; whether the transition state is further stabilized by π-donation from an adjacent phosphorus atom or donation of electron density from the aromatic ring is of less importance.

In summary, the current study reveals that the inversion behavior of trigonal pyramidal germanium(II) compounds is far from straightforward. In the compounds studied, in which a phosphorus substituent is directly bonded to the germanium center and in which a remote aromatic ring is present, several inversion mechanisms are possible. In each case inversion at germanium proceeds via an edge-inversion mechanism. It is apparent that the most important factor in the stabilization of such edge-inversion transition states is the σ-withdrawing nature of the substituents in the axial positions; π-donor effects are somewhat less important. In addition, our calculations have revealed for the first time that edge-inversion transition states may be stabilized by the donation of electron density from the π-system of a distal aromatic ring into the vacant p-orbital at the inversion center.

■ ASSOCIATED CONTENT

Supporting Information. Details of DFT calculations, final atomic coordinates, final energies, and details of imaginary frequencies for all geometries. This material is available free of charge via the Internet at http://pubs.acs.org.

■ AUTHOR INFORMATION

Corresponding Author
*E-mail: k.j.izod@ncl.ac.uk.

■ ACKNOWLEDGMENT

The authors are grateful to the EPSRC for support and acknowledge the use of the National Service for Computational Chemistry Software (NSCCS) in carrying out this work.

■ REFERENCES

(1) (a) Walsh, P. J.; Kozlowski, M. C. *Fundamentals of Asymmetric Catalysis*; University Science Books: Mill Valley, CA, 2009. (b) *Phosphorus Ligands in Asymmetric Catalysis*; Börner, A., Ed.; Wiley-VCH: Weinheim, Germany, 2008; Vol. 2; .

(2) Pelzer, S.; Wichmann, K.; Wesendrup, R; Schwerdtfeger, P. *J. Phys. Chem. A* **2002**, *106*, 6387.

(3) (a) Beachler, R. D.; Mislow, K. *J. Am. Chem. Soc.* **1970**, *92*, 4758. (b) Beachler, R. D.; Mislow, K. *J. Am. Chem. Soc.* **1971**, *93*, 773. (c) Beachler, R. D.; Casey, J. P.; Cook, R. J.; Senkler, G. H., Jr.; Mislow, K. *J. Am. Chem. Soc.* **1972**, *94*, 2859. (d) Beachler, R. D.; Andose, J. D.; Stackhouse, J.; Mislow, K. *J. Am. Chem. Soc.* **1972**, *94*, 8060.

(4) Driess, M.; Merz, K.; Monsé, C. *Z. Anorg. Allg. Chem.* **2000**, *626*, 2264.

(5) Dixon, D. A.; Arduengo, A. J.; Fukunaga, T. *J. Am. Chem. Soc.* **1986**, *108*, 2461.

(6) (a) Dixon, D. A.; Arduengo, A. J.; Roe, D. C. *J. Am. Chem. Soc.* **1986**, *108*, 6821. (b) Dixon, D. A.; Arduengo, A. J., III. *J. Am. Chem. Soc.* **1987**, *109*, 338. (c) Arduengo, A. J., III; Stewart, C. A.; Davidson, F.; Dixon, D. A.; Becker, J. Y.; Culley, S. A.; Mizen, M. B. *J. Am. Chem. Soc.* **1987**, *109*, 627. (d) Dixon, D. A.; Arduengo, A. J., III. *J. Chem. Soc., Chem. Commun.* **1987**, 498.

(7) (a) Schwerdtfeger, P.; Boyd, P. D. W.; Fischer, T.; Hunt, P.; Liddell, M. *J. Am. Chem. Soc.* **1994**, *116*, 9620. (b) Edgecombe, K. E. *J. Mol. Struct. (THEOCHEM)* **1991**, *226*, 157. (c) Creve, S.; Nguyen, M. N. *J. Phys. Chem. A* **1998**, *102*, 6549. (d) Moc, J.; Morokuma, K. *Inorg. Chem.* **1994**, *33*, 551. (e) Creve, S.; Nguyen, M. N. *Chem. Phys. Lett.* **1997**, *273*, 199. (f) Minyaev, R. M.; Wales, D. J.; Walsh, T. R. *J. Phys. Chem. A* **1997**, *101*, 1384. (g) Schwerdtfeger, P.; Hunt, P. *Adv. Mol. Struct. Res.* **1999**, *5*, 223. (h) Göller, A.; Clark, T. *Chem. Commun.* **1997**, 1033.

(8) Clotet, A.; Rubio, J.; Illas, F. *J. Mol. Struct. (THEOCHEM)* **1988**, *164*, 351.

(9) Izod, K.; McFarlane, W.; Allen, B.; Clegg, W.; Harrington, R. W. *Organometallics* **2005**, *24*, 2157.

(10) Izod, K.; Stewart, J.; Clark, E. R.; McFarlane, W.; Allen, B.; Clegg, W.; Harrington, R. W. *Organometallics* **2009**, *28*, 3327.

(11) (a) Becke, A. D. *J. Chem. Phys.* **1993**, *98*, 5648. (b) Stephens, P. J.; Devlin, F. J.; Chablowski, C. F.; Frisch, M. J. *J. Phys. Chem.* **1994**, *98*, 11623. (c) Hertwig, R. H.; Koch, W. *Chem. Phys. Lett.* **1997**, *268*, 345.

(12) (a) Hariharan, P. C.; Pople, J. A. *Theor. Chim. Acta* **1973**, *28*, 213. (b) Francl, M. M.; Petro, W. J.; Hehre, W. J.; Binkley, J. S.; Gordon, M. S.; DeFrees, D. J.; Pople, J. A. *J. Chem. Phys.* **1982**, *77*, 3654.

(13) (a) Peng, C.; Schlegel, H. B. *Isr. J. Chem.* **1993**, *33*, 449. (b) Peng, C.; Ayala, P. Y.; Schlegel, H. B.; Frisch, M. J. *J. Comput. Chem.* **1996**, *17*, 49.

(14) (a) Binkley, J. S.; Pople, J. A.; Hehre, W. J. *J. Am. Chem. Soc.* **1980**, *102*, 939. (b) Gordon, M. S.; Binkley, J. S.; Pople, J. A.; Pietro, W. J.; Hehre, W. J. *J. Am. Chem. Soc.* **1982**, *104*, 2797. (c) Pietro, W. J.; Francl, M. M.; Hehre, W. J.; Defrees, D. J.; Pople, J. A.; Binkley, J. S. *J. Am. Chem. Soc.* **1982**, *104*, 5039. (d) Dobbs, K. D.; Hehre, W. J. *J. Comput. Chem.* **1986**, *7*, 359. (e) Dobbs, K. D.; Hehre, W. J. *J. Comput. Chem.* **1987**, *8*, 861. (f) Dobbs, K. D.; Hehre, W. J. *J. Comput. Chem.* **1987**, *8*, 880.

(15) LeTourneau, H. A.; Birsch, R. E.; Korbeck, G.; Radkiewica-Poutsma, J. L. *J. Phys. Chem. A* **2005**, *109*, 12014.

(16) (a) Head-Gordon, M.; Pople, J. A.; Frisch, M. J. *Chem. Phys. Lett.* **1988**, *153*, 503. (b) Saebø, S.; Almlöf, J. *Chem. Phys. Lett.* **1989**, *154*, 83. (c) Frisch, M. J.; Head-Gordon, M.; Pople, J. A. *Chem. Phys. Lett.* **1990**, *166*, 275. (d) Frisch, M. J.; Head-Gordon, M.; Pople, J. A. *Chem. Phys. Lett.* **1990**, *166*, 281. (e) Head-Gordon, M.; Head-Gordon, T. *Chem. Phys. Lett.* **1994**, *220*, 122.

(17) (a) McLean, A. D.; Chandler, G. S. *J. Chem. Phys.* **1980**, *72* 5639. (b) Raghavachari, K.; Binkley, J. S.; Seeger, R.; Pople, J. A. *J. Chem. Phys.* **1980**, *72*, 650. (c) Binning, R. C., Jr.; L. Curtiss, A. *J. Comput. Chem.* **1990**, *11*, 1206. (d) McGrath, M. P.; Radom, L. *J. Chem. Phys.* **1991**, *94*, 511. (e) Curtiss, L. A.; McGrath, M. P.; Blaudeau, J.-P.; Davis, N. E.; Binning, R. C., Jr.; Radom, L. *J. Chem. Phys.* **1995**, *103*, 6104.

(18) Clark, T.; Chandrasekhar, J.; Spitznagel, G. W.; Schleyer, P. v. R. *J. Comput. Chem.* **1983**, *4*, 294.
(19) Pauling, L. *The Nature of the Chemical Bond*; Cornell University Press: New York, 1939.
(20) Bondi, A. *J. Phys. Chem.* **1964**, *68*, 441.
(21) (a) Batsanov, S. S. *Struct. Chem.* **1999**, *10*, 395. (b) Batsanov, S. S. *Russ. J. Coord. Chem.* **2001**, *27*, 890.
(22) (a) Carpenter, J. E.; Weinhold, F. *J. Mol. Struct. (THEOCHEM)* **1988**, *169*, 41.(b) Carpenter, J. E. Ph.D. Thesis, University of Wisconsin, Madison, WI, 1987. (c) Foster, J. P.; Weinhold, F. *J. Am. Chem. Soc.* **1980**, *102*, 7211. (d) Reed, A. E.; Weinhold, F. *J. Chem. Phys.* **1983**, *78*, 4066. (e) Reed, A. E.; Weinhold, F. *J. Chem. Phys.* **1985**, *83*, 1736. (f) Reed, A. E.; Weinstock, R. B.; Weinhold, F. *J. Chem. Phys.* **1985**, *83*, 735. (g) Reed, A. E.; Curtiss, L. A.; Weinhold, F. *Chem. Rev.* **1988**, *88*, 899.
(23) Albright, T. A.; Burdett, J. K.; Whangbo, M.-H. *Orbital Interactions in Chemistry*; Wiley: New York, 1985.
(24) Arduengo, A. J.; Dixon, D. A.; Roe, D. C.; Kline, M. *J. Am. Chem. Soc.* **1988**, *110*, 4437.
(25) (a) Yamamoto, Y.; Chen, X.; Akiba, K. *J. Am. Chem. Soc.* **1992***114*, 7906. (b) Yamamoto, Y.; Chen, X.; Kojima, S.; Ohdoi, K.; Kitano, M.; Doi, Y.; Akiba, K. *J. Am. Chem. Soc.* **1995**, *117*, 3922. (c) Akiba, K.; Yamamoto, Y. *Heteroatom Chem.* **2007**, *18*, 161.